International Journal of Software Engineering and Its Applications
Vol.8, No.4 (2014), pp.91-102
http://dx.doi.org/10.14257/ijseia.2014.8.4.11

# Fringe Analysis for Photoelasticity Using Image Processing Techniques

Tae Hyun Baek[1], Myung Soo Kim[2] and Dong Pyo Hong[3],

[1]*School of Mechanical and Automotive Engineering, Kunsan National University, Gunsan, Jeonbuk, 573-701, Korea,*
[2]*Dept. of Electronic Engineering, Kunsan National University, Gunsan, Jeonbuk, 573-701, Korea,*
[3]*School of Mechanical Engineering System, Chonbuk National University, Jeonju, Jeonbuk, 561-756, Korea*
*{thabek, mskim}@kunsan.ac.kr, hongdp@jbnu.ac.kr*

***Abstract***

*In research of photoelasticity, photoelastic fringe patterns are obtained through a circular polariscope with different optical arrangements and they are processed with image processing techniques in a personal computer. Image processing techniques are reviewed and discussed for stress analysis of the photoelastic fringes in this paper. The image processing techniques include fringe sharpening, fringe multiplication, and 8-step phase measuring technique. Gradient descent process is used for fringe sharpening. In fringe multiplication, fringes are multiplied twice for limited fringe order. 8-step phase measuring technique is used to separate isoclinics and isochromatics. The results of image processing techniques show that they are quite useful for stress analysis in photoelasticity.*

***Keywords:*** *Photoelasticity, Isoclinic Fringe, Isochromatic Fringe, Image Processing, Experimental Stress Analysis*

## 1. Introduction

Photoelasticity is widely used for stress analysis in mechanical engineering. Experiment in photoelasticity utilizes a polariscope that is an optical system [1, 2]. Birefringent phenomena of a photoelastic specimen in the polariscope make fringe patterns that depend on external load applied to the specimen. The fringe patterns are captured by CCD camera and saved in a computer. They are analyzed to obtain information about stress of the specimen. The polariscope takes advantages of the optical system that are two-dimensional signal process and non-contact measurement. This means that full-field measurement is available at once on the whole area of specimen through non-contact method in the photoelasticity experiment, compared with conventional point-by-point methods [2].

Fringe patterns obtained in the polariscope consist of broad fringe bands with different width and they have limited fringe orders. In this paper, image processing techniques are reviewed for better analysis of fringes in photoelasticity [3, 4]. Image sharpening technique is to locate easily maximum or minimum in the fringes [5]. Fringe multiplication technique is used to identify the 1/4 order fringes [6]. In addition, 8-step phase measuring technique is presented to separate isochromatics and isoclinics from the photoelastic fringes [7, 8]. All of algorithms in the techniques are implemented with

ISSN: 1738-9984 IJSEIA

Visual C++ of Microsoft that is convenient to use [9]. Through optical experiment, the techniques are applied to the photoelastic specimen for stress analysis and assessed.

## 2. Fringe Sharpening

Photoelasticity occurs when polarized light passes through a photoelastic specimen that is loaded. When one of principal stresses, $\sigma_3$, is zero for a plane stress problem, stress-optic law [1] is written with non-zero principal stresses, $\sigma_1$ and $\sigma_2$, as

$$\sigma_1 - \sigma_2 = \frac{N f_\sigma}{t}, \tag{1}$$

where $N$ is the isochromatic fringe order, $f_\sigma$ is the photoelastic constant for material and $t$ is the thickness of material. The function of polariscope is to determine the value of $N$ at each point on the specimen. In a circular polariscope with dark field arrangement [5], light intensity on the fringes, $I_D$, can be written

$$I_D = K \sin^2(\pi N), \tag{2}$$

where $K$ is a proportional constant that is the maximum light intensity on the fringes. Figure 1 shows the fringe pattern of the photoelastic specimen.

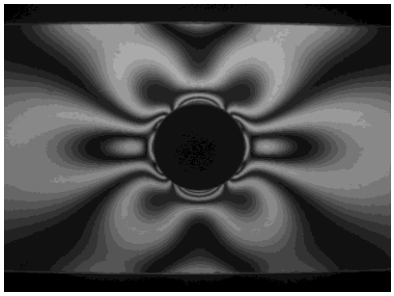

**Figure 1. Isochromatic Fringes by Dark Field Polariscope Set-Up Arrangement**

As seen in Figure 1, $I_D$ becomes 0 (totally black) for full-order fringes that are $N$ = 0, 1, 2, ⋯. On the other hand, $I_D$ becomes maximum $K$ (totally white) for half-order fringes that are N = 1/2, 3/2, 5/2, ⋯. It is not easy to locate clearly the extrema of half-order or full-order fringes, so that the sharpening process is used to get easily the information of extrema.

The sharpening algorithm based on gradient descent has been used in digital image processing [10]. To sharpen the fringes, measure of changes in a certain area for gradient descent, D, is used as follows:

$$D = K\left(1 - \frac{|\Sigma \nabla_x| + |\Sigma \nabla_y|}{\Sigma |\nabla_x| + \Sigma |\nabla_y|}\right), \tag{3}$$

where $\bigtriangledown_x$ and $\bigtriangledown_y$ are the $x$ and $y$-component of the gradient vector, respectively. There are no directional changes for $D$ = 0, so that the light intensities are changing uniformly. For $D = K$, the directional changes become maxima, so that the light intensities become local extrema.

 

| | | |
|---|---|---|
| *a* | *b* | *c* |
| *d* | *e* | *f* |
| *g* | *h* | *i* |

**Figure 2. Mask for Computing Gradient Descent**

A mask, as seen in Figure 2, is used to approximate the gradient values, and each component of the gradient vectors is calculated as follows:

$$\begin{aligned} \nabla_{x1} &= I_b - I_d, \quad & \nabla_{y1} &= I_a - I_e, \\ \nabla_{x2} &= I_c - I_e, \quad & \nabla_{y2} &= I_b - I_f, \\ \nabla_{x3} &= I_e - I_g, \quad & \nabla_{y3} &= I_d - I_h, \\ \nabla_{x4} &= I_f - I_h, \quad & \nabla_{y4} &= I_e - I_i. \end{aligned} \tag{4}$$

In Eqs. (4), $I_a$ is the light intensity at the pixel *a* in Figure 2, $I_b$ is the light intensity at the pixel *b*, and so on.

The sharpening process is applied to the fringe in Figure 1 and the result is in Figure 3(a). A comparison is made in Figure 3(b). The upper half pattern in Figure 3(b) is the upper half of original fringe of Figure 1 while the lower half pattern is the lower half of sharpened fringe of Figure 3(a). It is clear that the half- and full-order fringes are processed properly to sharpened lines.

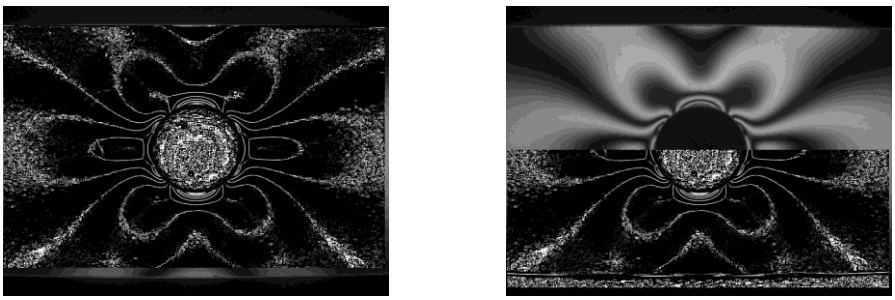

(a) (b)

**Figure 3. Results of Fringe Sharpening (a) Sharpened Fringes (b) Comparison of Before and After-Sharpening**

## 3. Fringe Multiplication

Fringes in photoelasticity can be multiplied for better analysis of stress. Light intensity on fringe pattern by the circular polariscope with light field arrangement, $I_L$, can be written

$$I_L = K \cos^2(\pi N). \tag{5}$$

For fringe multiplication, $I_R$ is taken as in Eq. (6),

$$I_R = | I_L - I_D | = | K \cos(2\pi N) |. \tag{6}$$

In Eq. (6), $I_R$ becomes 0 for $N$ = 1/4, 3/4, 5/4 $\cdots$, and becomes $K$ for $N$ = 0, 1/2, 3/2, This means that fringes are multiplied twice.

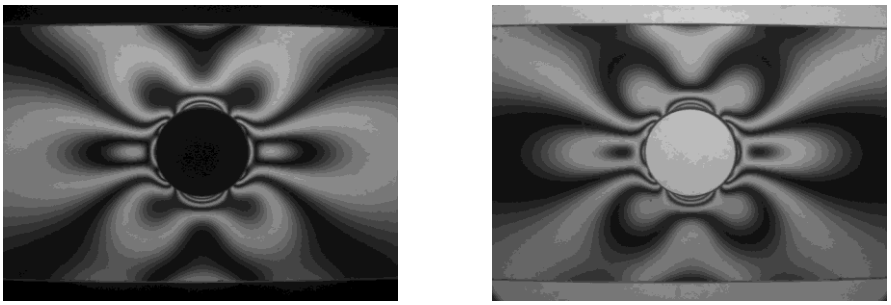

(a) (b)

**Figure 4. (a) Isochromatic Fringes in the Dark Field Polariscope Set-Up : $I_D$ (b) Isochromatic Fringes in the Light Field Fringes Set-Up : $I_L$**

The same specimen as for the fringe sharpening is used in the fringe multiplication. The fringes of $I_D$ and $I_L$ are in Figure 4. Multiplied fringes in Figure 5(a) are obtained by use of Eq. (6). To make sure of fringe multiplication, the upper half of multiplied fringes in Fig. 5(a) is sharpened and showed in the upper half of Figure 5(b) while the lower half of before-multiplied fringes in Figure 4(a) is sharpened and showed in the lower half of Figure 5(b). The effect of fringe multiplication is clearly visible along the local extrema through fringe sharpening as seen in Figure 5(b).

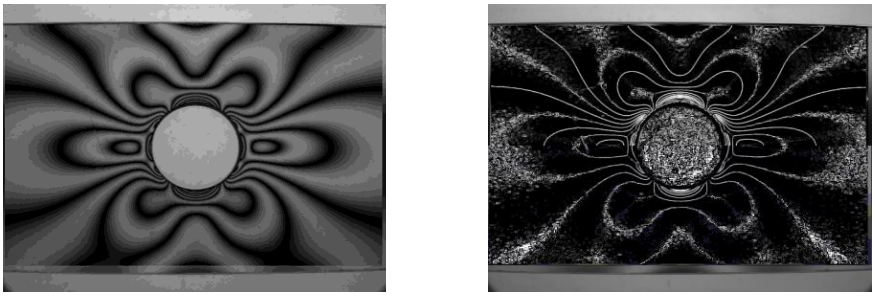

(a) (b)

**Figure 5. (a) Multiplied Fringes. (b) Comparison of After- and Before-multiplication in Fringes through Sharpening**

## 4. Measuring Technique for Separation of Isochromatics and Isoclinics

The method of photoelasticity allows one to obtain the principal stress directions and principal stress differences in the photoelastic specimen. The principal stress directions and the principal stress differences are provided by isoclinics and isochromatics, respectively. Conventionally, the principal stress directions are measured manually by rotating the polarizer and analyzer of a plane polariscope at the same time. This process is very tedious and time consuming in full-field analysis and it is usually difficult to separate isoclinics from photoelastic fringes. In this paper, 8-step phase measuring technique is used to separate isochromatics and isoclinics from photoelastic fringes through a circular polariscope and photoelastic experiments are performed to verify this technique.

 

### 4.1. Theory of Phase Measuring Technique

The schematic diagram of circular polariscope is in Figure 6. *P*, *Q*, *R* and *A* stand for polarizer, quarter-wave plate, stressed model (retarder) and analyzer. In Figure 6, the orientation of the element is written by a subscript which means the angle between the polarizing axis and the horizontal *x*-axis. The stressed model in Figure 6 means the photoelastic specimen that is loaded.

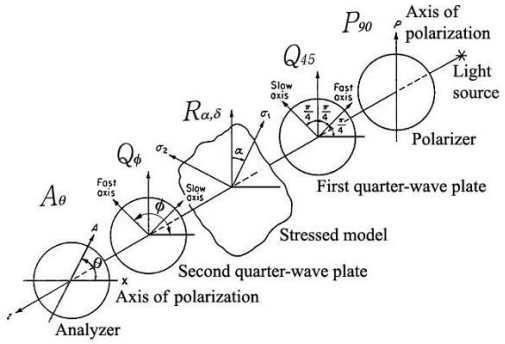


**Figur 6. Schematic Diagram of Circular Polariscope**

In Figure 6, $P_{90}$ indicates the polarizer whose transmission axis is perpendicular to the chosen x-axis. $Q_{45}$ indicates the first quarter-wave plate with fast axis at 45°. $R_{\alpha,\delta}$ stands for the stressed photoelastic specimen taken as a retardation $\delta$ and whose fast axis is at an angle $\delta$ with the x-axis. $Q_\varphi$ indicates the second quarter-wave plate with fast axis at $\phi$. $A_\theta$ indicates the analyzer whose transmission axis is $\theta$ to the chosen x-axis. Therefore by $P_{90}Q_{45}R_{\alpha,\delta}Q_\varphi A_\theta$, we mean ; ① the polarizer at 90°, ② the first quarter-wave plate with fast axis at 45°, ③ the specimen as retardation $\delta$ and whose fast axis is at an angle $\delta$ with the *x*-axis, ④ the second quarter-wave plate with fast axis at $\varphi$, and ⑤ the analyzer at $\theta$. A personal computer saves and processes the fringe pattern of 640 x 480 pixels with 8 bit intensity from CCD camera after the analyzer in Figure 6. The light source is monochromatic light of sodium lamp.

With the Jones calculus for the arrangement of $P_{90}Q_{45}R_{\alpha,\delta}Q_\varphi A_\theta$ in Fig. 6, the components of electric field in light from the analyzer [11] are given as

$$\begin{pmatrix} E_x \\ E_y \end{pmatrix} = \begin{bmatrix} \cos^2\theta & \sin\theta\cos\theta \\ \sin\theta\cos\theta & \sin^2\theta \end{bmatrix} \begin{bmatrix} i\cos^2\varphi + \sin^2\varphi & (i-1)\sin\varphi\ \cos\varphi \\ (i-1)\sin\varphi\ \cos\varphi & i\sin^2\varphi + \cos^2\varphi \end{bmatrix} \begin{bmatrix} e^{i\delta}\cos^2\alpha + \sin^2\alpha & (e^{i\delta}-1)\sin\alpha\ \cos\alpha \\ (e^{i\delta}-1)\sin\alpha\ \cos\alpha & e^{i\delta}\sin^2\alpha + \cos^2\alpha \end{bmatrix} \left(\frac{i+1}{2}\right) \begin{bmatrix} 1 & i \\ i & 1 \end{bmatrix} k\ e^{i\omega t}, \quad (7)$$

where $i = \sqrt{-1}$ and $\omega$ is the angular frequency of the light. The output light intensity is represented by

$$I = \bar{E}_x E_x + \bar{E}_y E_y . \quad (8)$$

In Eq. (8), $I$ is the output light intensity, and $\bar{E}_x$ and $\bar{E}_y$ are the complex conjugates of $E_x$ and $E_y$ that are the electric fields of light.

After the simple operation of Eq. (7) by Eq. (8), the output light intensity of the circular polariscope for the arrangement $P_{90}Q_{45}R_{\alpha,\delta}Q_\varphi A_\theta$ is given by

$$I = K\{1 - \sin 2(\theta - \varphi)\cos\delta - \sin 2(\varphi - \alpha)\cos 2(\theta - \varphi)\sin\delta\}, \quad (9)$$

where $K$ is a proportional constant, *i.e.*, the maximum light intensity emerging from the analyzer. For 8-phase measuring technique, the angle $\alpha$ and the relative retardation $\delta$ indicating the direction and the difference of principal stresses, respectively, are the parameters to be obtained.

**Table 1. Optical Arrangements and their 8 Fringe Patterns from Intensity Equations**

| No. | Arrangement | Output Intensity |
|---|---|---|
| 1 | $P_{90}Q_{45}R_{\alpha,\delta}Q_{45}A_{-45}$ | $I_1 = K(1 + \cos 2\alpha \sin\delta)$ |
| 2 | $P_{90}Q_{45}R_{\alpha,\delta}Q_{-45}A_{45}$ | $I_2 = K(1 - \cos 2\alpha \sin\delta)$ |
| 3 | $P_{90}Q_{45}R_{\alpha,\delta}Q_{-45}A_{0}$ | $I_3 = K(1 - \cos\delta)$ |
| 4 | $P_{90}Q_{45}R_{\alpha,\delta}Q_{45}A_{0}$ | $I_4 = K(1 + \cos\delta)$ |
| 5 | $P_{90}Q_{45}R_{\alpha,\delta}Q_{0}A_{0}$ | $I_5 = K(1 + \sin 2\alpha \sin\delta)$ |
| 6 | $P_{90}Q_{45}R_{\alpha,\delta}Q_{90}A_{90}$ | $I_6 = K(1 - \sin 2\alpha \sin\delta)$ |
| 7 | $P_{90}Q_{45}R_{\alpha,\delta}Q_{0}A_{45}$ | $I_7 = K(1 - \cos\delta)$ |
| 8 | $P_{90}Q_{45}R_{\alpha,\delta}Q_{90}A_{45}$ | $I_8 = K(1 + \cos\delta)$ |

In 8-step phase measuring technique, the output intensities of eight images are used as in Table 1. For instance, the intensity $I_1$ of No. 1 arrangement in Table 1 can be obtained from Eq. (9) for $\theta$=−45° and $\phi$=45°. The optical arrangements of Table 1 are similar to those of Ref. [12]. However, the polarizer and the first quarter wave plate as in Figure 6 and Table 1 are fixed with angles 90 and 45 degrees, respectively, from the $x$-axis in these arrangements. These arrangements are simple to use and take short time in actual data-acquisition.

The equations shown in Table 1 are used for the calculations of isoclinic $\alpha$ and fractional fringe order $\delta$ [6] as

$$\alpha = \frac{1}{2}\tan\left(\frac{I_5 - I_6}{I_1 - I_2}\right), \quad (10)$$

$$\delta = \tan^{-1}\left\{\frac{(I_1 - I_2)\cos 2\alpha + (I_5 - I_6)\sin 2\alpha}{\frac{1}{2}\{(I_4 - I_3) + (I_8 - I_7)\}}\right\}. \quad (11)$$

### 4.2. Simulation Test of 8-Step Phase Measuring Technique

A feasibility study using computer simulation is done to separate isoclinics and isochromatics from photoelastic fringes of a circular disk under diametric compression. The radius and the thickness of the disk used in the simulation test are 3.81 cm and 0.476 cm, respectively. Diametrical compression load, $P$=26.7 N, is applied to the disk. Material fringe constant, $f_\sigma$ = 5.254 N/cm, is used. From the given conditions, theoretical value of isochromatic $\delta$ is related to two principal stress components, $\sigma_1$ and $\sigma_2$, as in Eq. (12). On the other hand, theoretical isoclinic angle $\alpha$ can be calculated by Eq. (13) using stress components, $\sigma_x$, $\sigma_y$, and $\tau_{xy}$.

 

$$\delta = \frac{2\pi t}{f_\sigma}(\sigma_1 - \sigma_2), \tag{12}$$

$$\alpha = \frac{1}{2}\tan^{-1}\left[\frac{\tau_{xy}}{(\delta_x - \delta_y)/2}\right]. \tag{13}$$

From the simulated eight images of the circular disk [6], isoclinic phase map using Eq. (10) can be obtained as in Fig. 7. Fig. 7 is used to yield isochromatic phase map as in Fig. 8. The fringe phases on phase maps in Fig. 7 and Fig. 8 are wrapped fringe phases. In order to get continuous distributions and/or physical quantities, the values at the phase jump are connected by means of unwrapping procedure. Fig. 9 shows wrapped and unwrapped isochromatic phase distributions along the same line A-A as indicated in Fig. 8.


**Figure 7. Phase Maps of Isoclinic from Simulation of a Disk under Diametric Compression**

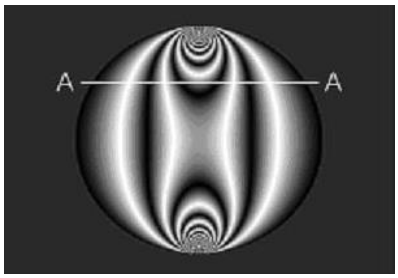


**Figure 8. Phase Maps of Isochromatics using Figure 7**

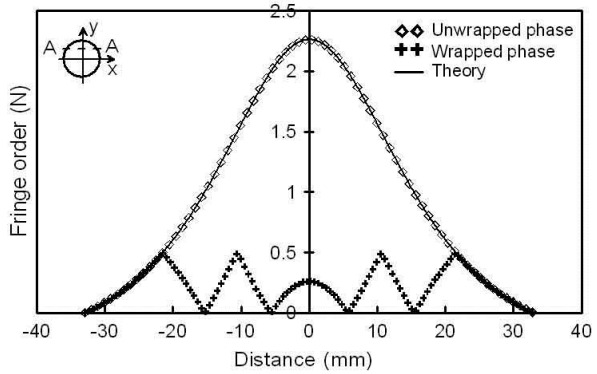


**Figure 9. Distributions of Unwrapped and Wrapped Isochromatic Phase Map along line A-A of Figure 8**

In Figure 10, the distributions of wrapped isoclinic phase map along the horizontal line A-A is shown. As shown in Figure 10, the phases of isoclinics are changed when $I_1=I_2=I_5=I_6$ in Table 1, which occur when $\delta$ = 0, $\pi$, $2\pi$, *etc*. The phase changes of isoclinics in Fig. 10 can be eliminated after unwrapping isochromatic phase, which represents $\delta$ as in Figure 9. The distributions of unwrapped isoclinic phase are shown in Figure 11, and they are exactly agreed to those of theories calculated by Eq. (13).

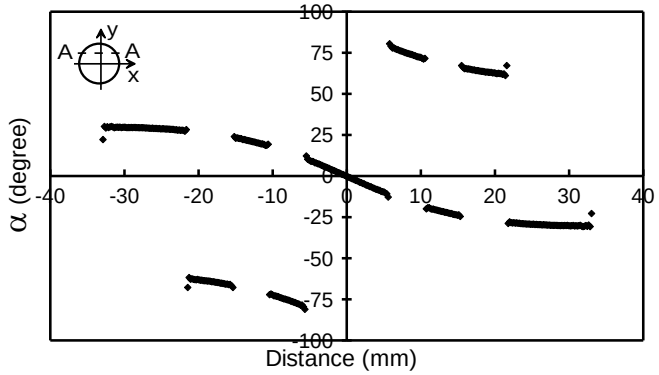


**Figur 10. Distributions of Wrapped Isoclinic Phase Map along Line A-A of Figure 7**

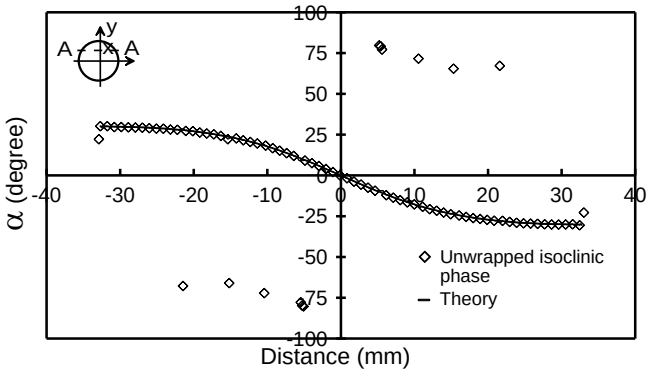


**Figure 11. Distributions of Wrapped Isoclinic Phase Map along Line A-A of Figure 7 using Unwrapped Isochromatics of Figure 9**

However, big errors occur at or near the centers of isochromatic fringes. These errors can be easily recognized and taken off by simple image processing. All the results in Figures 9 through 11 are calculated with the simulated images of the circular disk. Therefore, it is verified that the procedure for the separation of isochromatics and isoclinics from photoelastic fringes used in the simulation is valid.

### 4.3. Assessment of 8-Step Phase Measuring Technique

To assess the practical use of the developed method in this work, a stress-frozen disk under diametric compression, 45.2 mm in diameter and 4.0 mm thick made of epoxy, is used as the photoelastic specimen in the circular polariscope of Figure 6. Material fringe value and applied load at the stress freezing point are $f_\sigma$ = 0.3517 kN/m and $P$ = 36.15 N, respectively.

 

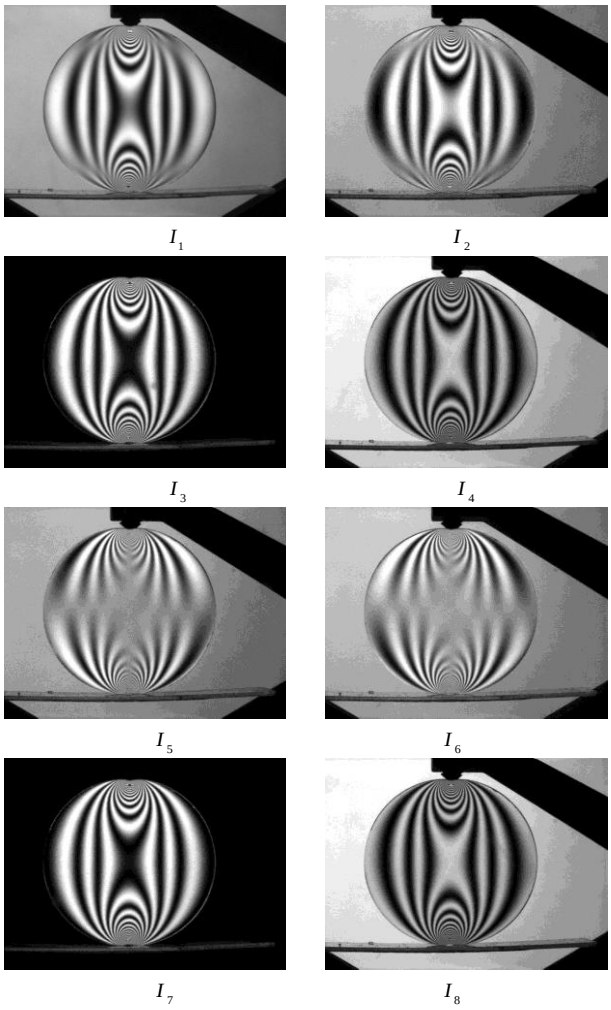


**Figure 12. Eight Images Obtained by the Optical Arrangements of Table 1**

Eight images in Table 1 are obtained by photoelastic experiment as shown in Figure 12. Isoclinic phase map using Eq. (8) is shown in Figure 13(a). This isoclinic phase map of Fig. 13(a) is directly used for the calculation of isochromatic phase as shown in Figure 13(b). In order to check the distributions of isochromatics quantitatively, unwrapped phase in Figure 14 is obtained from the wrapped phase of isochromatics along a line A-A across the middle point of the upper half disk as shown in Figure 13(b). Note that the wrapped phases of isochromatics in Figure 14 are directly obtained from the wrapped isoclinic phases shown in Figure 13(a). Generally, unwrapping of wrapped isoclinics should be prerequisite to get wrapped isochromatic phases.

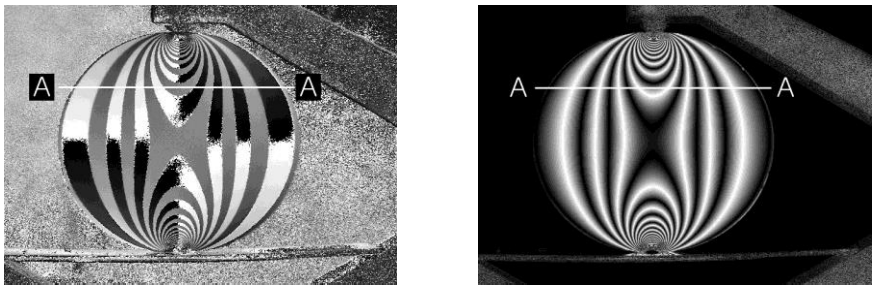


(a) (b)

**Figure 13. Wrapped Phases of (a) Isoclinics and (b) Isochromatics**

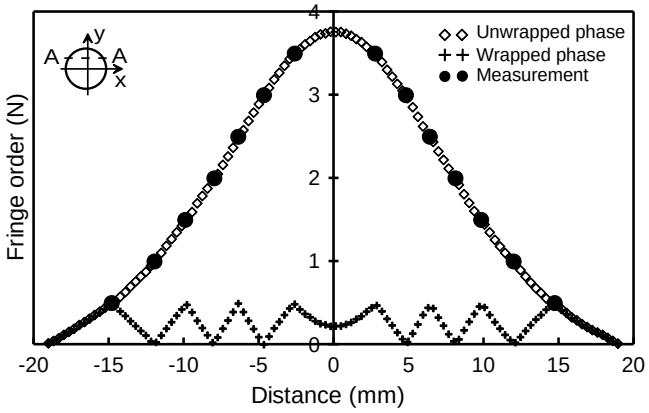


**Figure 14. Unwrapped and Wrapped Isochromatic Phase Distributions along Line A-A Indicated in Figure 13(b)**

In this research, it is not required to unwrap isoclinic phase for the calculations of isochromatics [8]. Also, it is possible to exclude possible errors due to numerical calculation and/or digitization for unwrapping isoclinics. The experimental results obtained from unwrapped isochromatics are exactly agreed to the manual measurements at the fringe centers as shown in Figure 14. Figure 15 shows the wrapped isoclinic distributions along a line A-A in Figure 13(a). The unwrapped isoclinic phases of Figure 16 can be obtained by using unwrapped isochromatics of Figure 14.

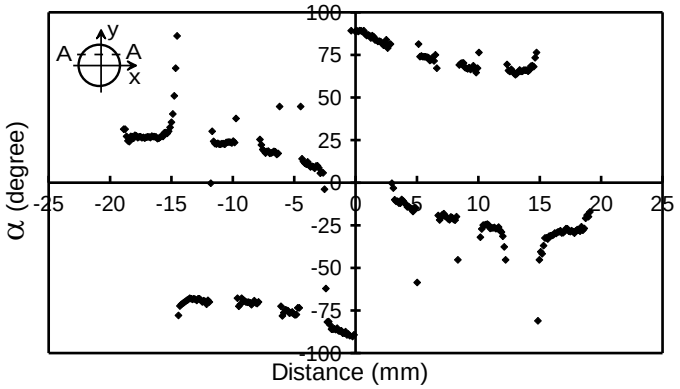


**Figure 15. Wrapped Isoclinic Phase Distributions along Line A-A Indicated in Figure 13(a)**

 

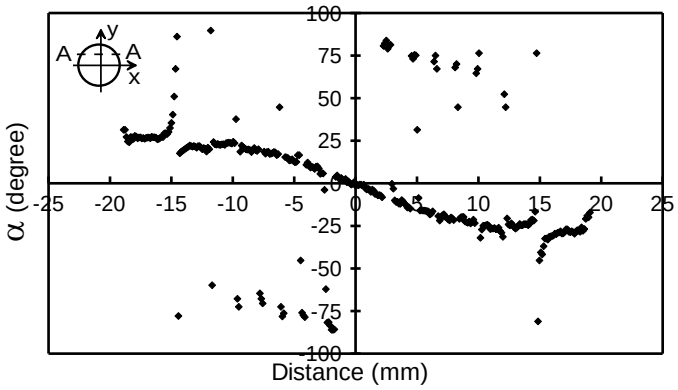


**Figure 16. Unwrapped Isoclinic Distribution along Line A-A Indicated in Figure 13(a)**

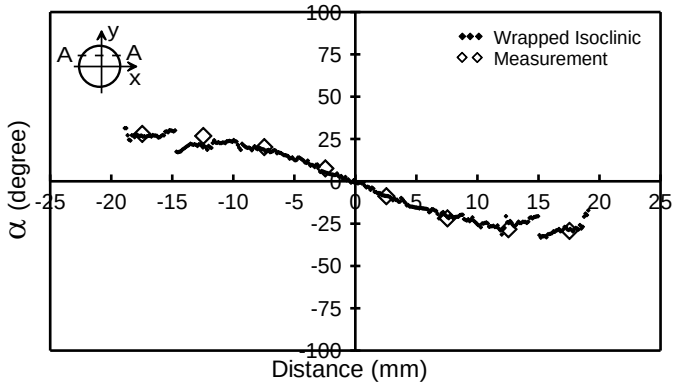


**Figure 17. Comparisons of Isoclinic Distributions by 8-step Phase Measuring Technique and Manual Measurements along Line A-A Indicated in Figure 13(a)**

In other words, unwrapping isoclinics are done after unwrapping isochromatics. Unexpected big errors occur at or near the centers of isochromatics. These errors can easily be recognized and eliminated by means of appropriate image processing. Results of the isoclinics along the line A-A in Figure 13(a) are compared with those determined by the manual measurements in Figure 17. Again, it is observed that the unwrapped isoclinics obtained by 8-step phase measuring technique are close to manual measurements.

## 5. Conclusion

Photoelasticity is a reliable optical technology for stress analysis in mechanics. Advance in a personal computer has facilitated use of photoelastic techniques. In this paper, image processing techniques are applied to stress analysis of fringes in photoelastic specimen. Gradient descent process is successfully used for the sharpening technique on the fringes. The fringes are multiplied twice for limited fringe order by use of dark- and light-field fringes. The fringe multiplication is confirmed with the sharpening technique of fringes. In addition, 8-step phase measuring technique is shown to separate isoclinics and isochromatics. The validity of 8 step phase measuring

technique for separation of isoclinics and isochromatics is proved by use of photoelastic experiment.

## Acknowledgements

This research was supported by Basic Science Research Program through the National Research Foundation of Korea (NRF) funded by the Ministry of Education, Science and Technology (Grant number: 2013-070058).

## References

[1] J. W. Dally and W. F. Riley, "Experimental Stress Analysis", 2nd Ed., McGraw-Hill Inc., **(1991)**.
[2] G. L., "Cloud, Optical Methods of Engineering Analysis", Cambridge University Press, **(1998)**.
[3] T. H. Baek, M. S. Kim and D. P. Hong, Advanced Science and Technology Letters, (Signal Processing), Jeju Island, Korea, vol. 37, **(2013)** December 11-13, pp. 5-8.
[4] K. Ramesh, T. Kasimayan and B. Simon, J. of Strain Analysis for Engineering Design, vol. 46, no. 4, **(2011)**, pp. 245-266.
[5] T. H. Baek and M. S. Kim, Proc. of 1993 SEM 50th Anniversary, Spring Conference on Experimental Mechanics, Bethel, Connecticut, USA, **(1993)**. pp. 674-681.
[6] T. H. Baek and J. C. Lee, Transactions of the KSME, vol. 18, no. 10, **(1994)**, pp. 2577-2584.
[7] T. H. Baek, M. S. Kim and S. H. Cho, J. of the Korean Society for Nondestructive Testing, vol. 21, no. 2, **(2001)**, pp. 189-196.
[8] T. H. Baek, M. S. Kim, Y. Morimoto and M. Fugigaki, KSME International J., vol. 16, no. 2, **(2002)**, pp. 1207-1213.
[9] Microsoft Visual C++ 6.0, Microsoft Corporation, USA, **(1998)**.
[10] R. Gonzalez and R.Woods, Digital Image Processing, 3rd Ed., Prentice Hall, **(2007)**.
[11] P. E. Theocaris and E. Gdoutos, Matrix Theory of Photoelasticity, Springer-Verlag, **(1979)**.
[12] J. A. Quiroga and A. Gonzales-Cano, Applied Optics, vol. 36, no. 2, **(1997)**, pp. 8397-8402.

 